Supporting Information for: *Towards Pareto optimal high entropy alloy hydrides via data-driven materials discovery*

Matthew Witman*[1], Sanliang Ling[2], Matthew Wadge[2], Anis Bouzidi[3], Nayely Pineda-Romero[3], Rebecca Clulow[4], Gustav Ek[4], Jeffery Chames[1], Emily Allendorf[1], Sapan Agarwal[1], Mark Allendorf[1], Gavin S. Walker[2], David Grant[2], Martin Sahlberg[4], Claudia Zlotea[3] and Vitalie Stavila*[1]

[1]Sandia National Laboratories, Livermore, California 94551, USA
[2]Advanced Materials Research Group, Faculty of Engineering, University of Nottingham, University Park, Nottingham, NG7 2RD, UK
[3]Univ Paris Est Créteil, CNRS, ICMPE, UMR 7182, 2 rue Henri Dunant, 94320, Thiais, France
[4]Department of Chemistry - Ångström Laboratory, Uppsala University, Box 523, SE-75120, Uppsala, Sweden

S1. ML-ready HydPARK augmentation with HEA hydride thermodynamics

v0.0.4 of the ML-HydPARK database[1] was supplemented with thermodynamic properties of hydrides investigated for thermal hydrogen compression as summarized in Refs. 2 and 3, as well as the HEA hydride measurements we collected from the recent literature in Table S1. The jupyter notebook to reproduce these results is provided at `https://github.com/mwitman1/HEAhydrideMLv2`, and the scikit-learn gradient boosting regressor hyperparameters utilized were: {'n_estimators'=1500, 'learning_rate'=0.005, 'learning_rate'=0.005, 'max_depth'=4, 'subsample'=0.75, 'alpha'=0.99}.

Composition	ΔH	ΔS	$\ln\left(P^o_{eq}/P_o\right)$	Hwt.%	H/M	T	Reference
NbTiVZrHf	61.8	88.0	-14.35	2.2	2.06	315.0	Ref. 4
VTiZrNb	67.6	90.3	-16.41	1.5	1.07	311.0	Ref. 5
$NbTiV_{0.5}ZrHf$	59.1	87.4	-13.33	1.8	1.76	326.0	Ref. 5
VTiAlCr	42.7	88.4	-6.59	1.1	0.49	311.0	Ref. 6
VTiAlTaNb	56.1	92.1	-11.55	1.25	1.0	301.0	Ref. 6
TiVCrNb	47.1	122.0	-4.33	3.0	1.87	100.0	Ref. 7
$Al_{0.1}Ti_{0.3}V_{0.3}Nb_{0.3}$	48.6	154.0	-1.08	2.6	1.59	62.5	Ref. 8

Table S1: HEA hydride thermodynamic data from recent literature.

*mwitman@sandia.gov ; vnstavi@sandia.gov

S2. DFT settings

All density functional theory (DFT) calculations, including structural optimizations and total energy calculations, were performed using the Vienna Ab initio Simulation Package.[9] We used a plane-wave basis set with a kinetic energy cutoff of 400 eV to expand the wave functions, and the Perdew-Burke-Ernzerhof functional[10] with the projector augmented wave method[11,12] were used to solve the Kohn-Sham equations. A first-order Methfessel-Paxton smearing[13] with a width of 0.2 eV was used to improve the convergence of electronic self-consistent field calculations. All DFT calculations have been performed using a k-point mesh with a spacing of ca. 0.20 $Å^{-1}$. An energy convergence threshold of 10^{-4} eV was used for all total energy calculations. Due to the large number of structures that need to be considered, a relatively loose structural optimization convergence criterion was used, where the structural optimizations, including cell parameters and atomic positions, were considered converged if all interatomic forces fall below 0.05 eV/Å.

S3. H_2 desorption characterization

Hydrogen can be desorbed from the RBM synthesized FCC hydrides by heating to 450 °C under secondary vacuum, thereby demonstrating reversible reaction with hydrogen, as shown by the thermal desorption spectroscopy (TDS) measurements in Figure S1. The desorbed phases adopt a BCC lattice ($Im\bar{3}m$) in Figure S1, as expected for these materials. Peak refinement yields the lattice parameters of 3.404(5) Å, 3.155(8) Å, and 3.067(2) Å for MgTiVNbZrHf, MgTiVCrNb, and MgAlTiVCr respectively, which is consistent with the trend of FCC hydride lattice parameters in the main text. These values are compared to the DFT-relaxed BCC configurations described in the main text in Table S2. The DFT-relaxed, dihydride FCC (H/M = 2) random alloy configurations for each composition visualize slight distortions to metal and tetrahedral hydrogen locations arising from local strain induced by the random metal ordering in the HEA lattice (Figure S2).

Composition	Experiment	DFT
MgTiVNbZrHf	19.7	19.1
MgTiVCrNb	15.7	16.2
MgAlTiVCr	14.4	15.6

Table S2: Volume per atom of the experimentally resolved BCC alloys and the DFT relaxed random alloy configuration.

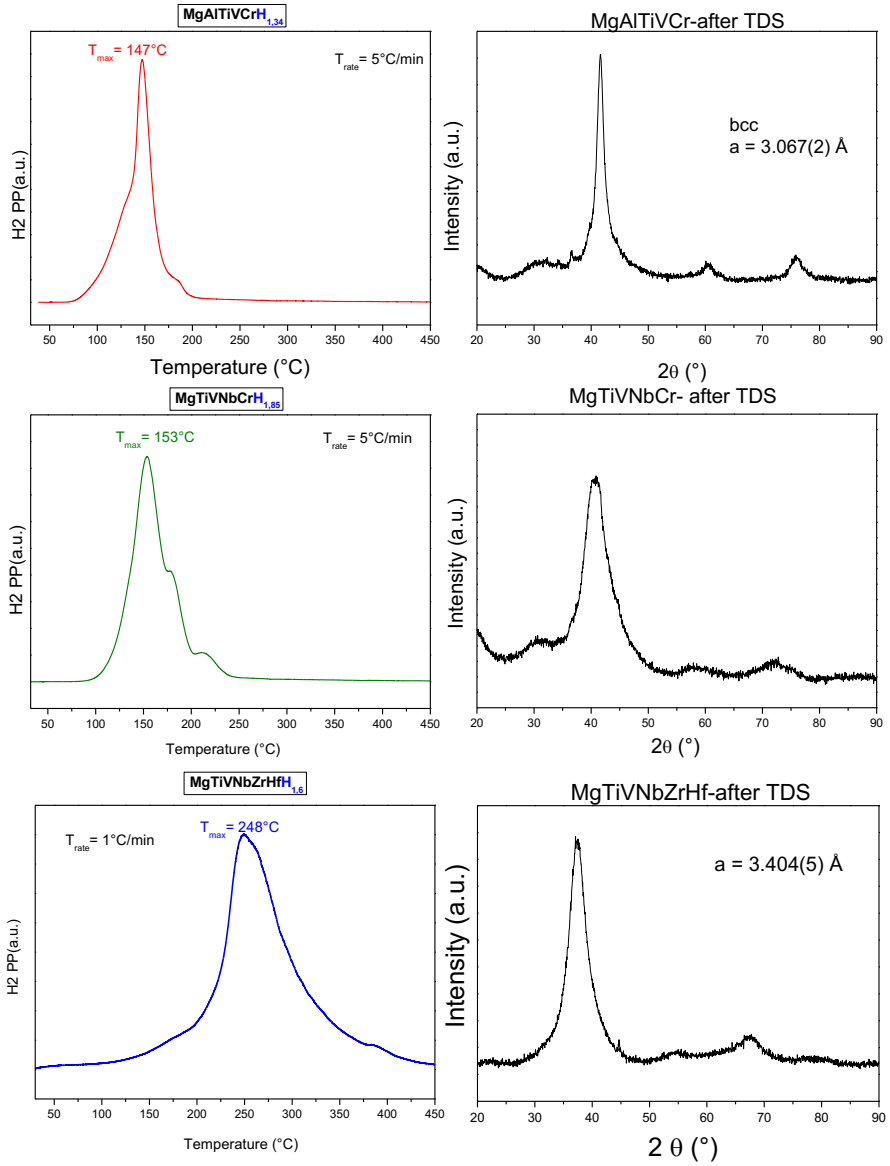

Figure S1: TDS of as synthesized FCC hydrides and XRD of the dehydrogenated BCC alloy phase.

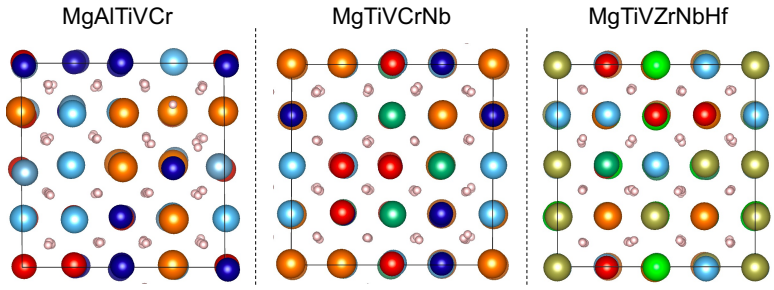

Figure S2: DFT-relaxed, dihydride (H/M = 2) FCC alloy configurations for each composition.

S4. MgTiVCrNb PCT measurements

Due to sluggish kinetics and a highly sloped plateau of MgTiVCrNb, the hydriding thermodynamics could only be extracted by measuring the full PCT curves at 644 K, 654 K and 664 K for the van't Hoff analysis, rather than the method used for MgAlTiVCr and MgTiVZrNbHf. The isotherms at each temperature and corresponding van't Hoff plot (inset) are shown in Figure S3. The experimental uncertainty in the van't Hoff analysis is high ($\Delta H = 68 \pm 9$ kJ/molH_2) due the highly sloped plateau of this sample and limited range of temperatures where the PCT isotherms could be collected. If one performs a van't Hoff analysis using only the two highest temperature and two lowest temperature PCT curves, one obtains widely varying ΔH predictions of 52 or 82 kJ/molH_2, which are below and above the ML prediction, respectively.

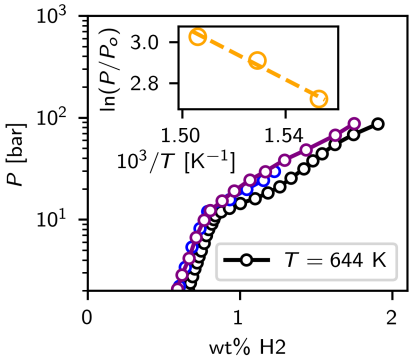

Figure S3: PCT curves for MgTiVCrNb are shown with black, blue, and purple corresponding to 644 K, 654 K, and 664 K measurements, respectively. The inset shows the pressure vs. inverse temperature points used in the van't Hoff analysis.

S5. EDS Spectra

EDS spectrum corresponding to the EDS maps in the main manuscript (after H_2 cycling) are shown in Figure S4. The EDS spectra confirm the elemental composition of the HEA samples. The small amounts of iron present are from the ball-milling hardware.

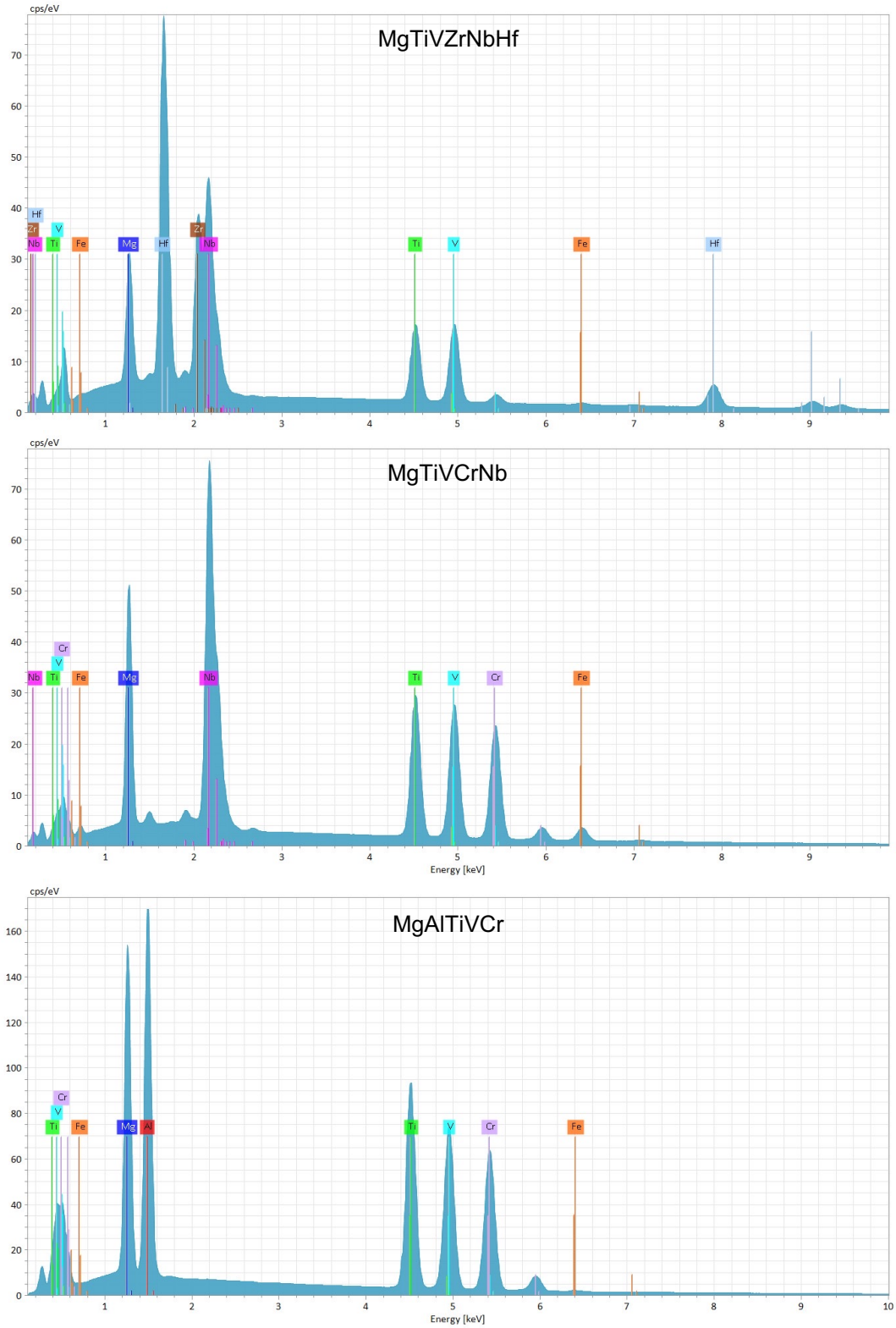

Figure S4: EDS spectra for MgTiVNbZrHf, MgTiVNbCr, and MgAlTiVCr after H_2 cycling.

References

[1] M. Witman, M. Allendorf, and V. Stavila, "Database for machine learning of hydrogen stroge materials properties (0.0.4) [Data set]," 2022.

[2] M. Lototskyy, V. Yartys, B. Pollet, and R. Bowman, "Metal hydride hydrogen compressors: A review," *Int. J. Hydrogen Energy*, vol. 39, pp. 5818–5851, apr 2014.

[3] J. Bellosta von Colbe, J.-R. Ares, J. Barale, M. Baricco, C. Buckley, G. Capurso, N. Gallandat, D. M. Grant, M. N. Guzik, I. Jacob, E. H. Jensen, T. Jensen, J. Jepsen, T. Klassen, M. V. Lototskyy, K. Manickam, A. Montone, J. Puszkiel, S. Sartori, D. A. Sheppard, A. Stuart, G. Walker, C. J. Webb, H. Yang, V. Yartys, A. Züttel, and M. Dornheim, "Application of hydrides in hydrogen storage and compression: Achievements, outlook and perspectives," *Int. J. Hydrogen Energy*, vol. 44, pp. 7780–7808, mar 2019.

[4] M. Sahlberg, D. Karlsson, C. Zlotea, and U. Jansson, "Superior hydrogen storage in high entropy alloys," *Sci. Rep.*, vol. 6, p. 36770, dec 2016.

[5] G. Ek, M. M. Nygård, A. F. Pavan, J. Montero, P. F. Henry, M. H. Sørby, M. Witman, V. Stavila, C. Zlotea, B. C. Hauback, and M. Sahlberg, "Elucidating the Effects of the Composition on Hydrogen Sorption in TiVZrNbHf-Based High-Entropy Alloys," *Inorg. Chem.*, vol. 60, pp. 1124–1132, jan 2021.

[6] M. Witman, G. Ek, S. Ling, J. Chames, S. Agarwal, J. Wong, M. D. Allendorf, M. Sahlberg, and V. Stavila, "Data-Driven Discovery and Synthesis of High Entropy Alloy Hydrides with Targeted Thermodynamic Stability," *Chem. Mater.*, vol. 33, pp. 4067–4076, jun 2021.

[7] M. M. Nygård, Ø. S. Fjellvåg, M. H. Sørby, K. Sakaki, K. Ikeda, J. Armstrong, P. Vajeeston, W. A. Sławiński, H. Kim, A. Machida, Y. Nakamura, and B. C. Hauback, "The average and local structure of $TiVCrNbD_x$ (x=0;2:2;8) from total scattering and neutron spectroscopy," *Acta Mater.*, vol. 205, p. 116496, feb 2021.

[8] N. Pineda-Romero, M. Witman, V. Stavila, and C. Zlotea, "The effect of 10 at.% Al addition on the hydrogen storage properties of the Ti0.33V0.33Nb0.33 multi-principal element alloy," *Intermetallics*, vol. 146, p. 107590, jul 2022.

[9] G. Kresse and J. Furthmüller, "Efficient iterative schemes for ab initio total-energy calculations using a plane-wave basis set," *Phys. Rev. B*, vol. 54, pp. 11169–11186, Oct. 1996.

[10] J. P. Perdew, K. Burke, and M. Ernzerhof, "Generalized gradient approximation made simple," *Phys. Rev. Lett.*, vol. 77, pp. 3865–3868, Oct. 1996.

[11] P. E. Blöchl, "Projector augmented-wave method," *Phys. Rev. B*, vol. 50, pp. 17953–17979, Dec. 1994.

[12] D. Hobbs, G. Kresse, and J. Hafner, "Fully unconstrained noncollinear magnetism within the projector augmented-wave method," *Phys. Rev. B*, vol. 62, pp. 11556–11570, Nov. 2000.

[13] M. Methfessel and A. T. Paxton, "High-precision sampling for brillouin-zone integration in metals," *Phys. Rev. B*, vol. 40, pp. 3616–3621, Aug. 1989.